# Hybridized Local and Charge Transfer Modulated Triplet Decay Brightens Ultra-Long Circularly Polarized Afterglow and Chiral Diradical Activity

**Bo Yang[1], Suqiong Yan[1], Hui Ma[1], Shirong Ban[1], Yuan Zhang[1], Fanda Feng,[1] and Wei Huang[1,2]***

**ABSTRACT: The design and construction of chiral phosphors with significant long-lived triplet exciton decay have received great attention because of their prospective applications in ultra-long circularly polarized room-temperature phosphorescence (CP-RTP) for chiral optics. However, the practical utilization of pure organics as triplet incubators is often hindered by their spin-forbidden transition. Therefore, it is a substantial challenge for the developments of organic-derived CP-RTP emitters with both long lifetimes and asymmetry factors. Herein, via precisely manipulating hybridized local and charge transfer (HLCT) and multiple n−π* effects, we report the first P,N-embedded tactic to construct the BINAP-derived emitters, which show tunable circularly polarized luminescence (CPL) with high photoluminescence quantum efficiency (up to 95%), $|g_{lum}|$ values (1.2 to 6.2 × $10^{-3}$), and ultra-long RTP with remarkable lifetime as long as 448 ms in the polymethyl methacrylate. Experiments and quantum chemistry simulations unveil that the above-mentioned triplet decay is derived from tunable HLCT and a balanced electric-magnetic dipole moment environment. Moreover, the synergetic enhancement of chemical and configurational stability enables stable chiral diradicals with a high diradical character ($y_0$ = 0.953) and Near-Infrared Ray (NIR) optical activity. This work provides important clues for CP-RTP phosphors and chiral diradical materials from phosphine chemistry.**

## INTRODUCTION

Designing and constructing novel chiral luminophores with triplet exciton populations are stepping-stones for chiral photo-electro-magnetic materials, such as circularly polarized organic light-emitting diodes (CP-OLEDs),[1–6] ultra-long CP-RTP,[7–11] chirality-induced spin electronics,[12] and triplet photosensitizers.[13] Among the available emissive building precursors for constructing desired CPL, binaphthyl derivates have attracted tremendous attention over the past decades because of their remarkable structural diversity as well as high stereochemical stability (Figure 1a).[4,14–17] However, triplet population and utilization by exclusive binaphthyl-derived molecules are particularly unsatisfying for single-molecular CP-RTP because of limited spin-flipping via the $^1\pi-\pi^* \rightarrow {}^3\pi-\pi^*$ conversion during the intersystem crossing process (ISC).[3,10,18]

In this background, constructing donor-acceptor (D−A) molecular knots has been utilized to establish the prominent electron-hole pair separation and a small single-triplet energy gap ($\Delta E_{ST} \leq 0.3$ eV), leading to the additional intermolecular charge transfer (ICT) and dominant $^1CT \leftrightarrow {}^3CT$ shuttling.[19,20] The higher ISC speed and small $\Delta E_{ST}$ will enable the reverse ISC (RISC) possibility for realizing thermally activated delayed fluorescence (TADF) instead of ultra-long RTP at room temperature.[20–22] Despite all this, the inherent spin-forbidden transition in the $S_n \leftrightarrow T_n$ is still present because of the small spin-orbit coupling coefficient ($\zeta_{soc}$) in most organics.[23,24] Hence, the doping of heteroatoms (N, O, P, S, B, Br, and I)[25–29] and heavy-atoms (Ir, Pt, Au, Cu et al)[30–32] has been proposed to realize effective $\zeta_{soc}$ on the basis of the El-Sayed rule. The former heteroatom doping has dominance in the balanced phosphorescent efficiency, RTP lifetime, and low cost.

At present, many chiral-emitting blocks are still under development. For instance, the D−A chiral emitters of triazine/cyano-decorative carbazoles and B-N multiple resonance structures have been widely explored in their circularly polarized TADF (CP-TADF) activity in recent years (Figure 1a).[1–6] In this context, how to selectively balance the emission decay, quantum efficiency, and asymmetry factors has been the current research focus.[27–32] Generally, superior luminescence efficiencies often accompany deteriorated dissymmetry factors in CPL, which is mainly caused by the near-vertical angle of electro-magnetic dipole moment ($\theta_{e\text{-}m}$) from unsatisfactory chiral excited states. This physical connotation is quantified by the formal of $g = 4\ |\mu_e| \times |\mu_m| / (|\mu_e|^2 + |\mu_m|^2) \times \cos\theta_{e\text{-}m}$, where the $\theta_{e\text{-}m}$ is crucial for the CPL optimization.[6,39] Unfortunately, the sophisticated TADF emitters are known to output both fast ISC and RISC processes in the excited states at room temperature due to predominant intramolecular $^1CT \leftrightarrow {}^3CT$ progress, which do not apply to pursue long-lived triplet resident and radiation for ultra-long CP-RTP. Therefore, further exploration should be considered for the phosphorescence emitters with CP-RTP in monocomponent organics.[40–43]

In the continuous advances, chiral multi-component assembly and single-molecular tailoring tactics have received great dedication in mechanism investigation and application exploitation.[7,17,42] In fact, phosphine is a variable valency unit for modulated electronic structures (Figure 1b).[44] Recently, our team reported the selective ISC output in P,O-atoms embedded SEGPHOS for CP-RTP in single crystals, but the weak emission and RTP are annihilated in solution and amorphous state at room temperature.[25] Unfortunately, this nonluminous disadvantage exists extensively in conventional chiral phosphine ligands, where the molecular design is considered from the catalytic perspective rather than

[1]State Key Laboratory of Coordination Chemistry, School of Chemistry and Chemical Engineering, Nanjing University, Nanjing 210093, P. R. China. E-mail: whuang@nju.edu.cn
[2]Shenzhen Research Institute of Nanjing University, Shenzhen 518057, P. R. China

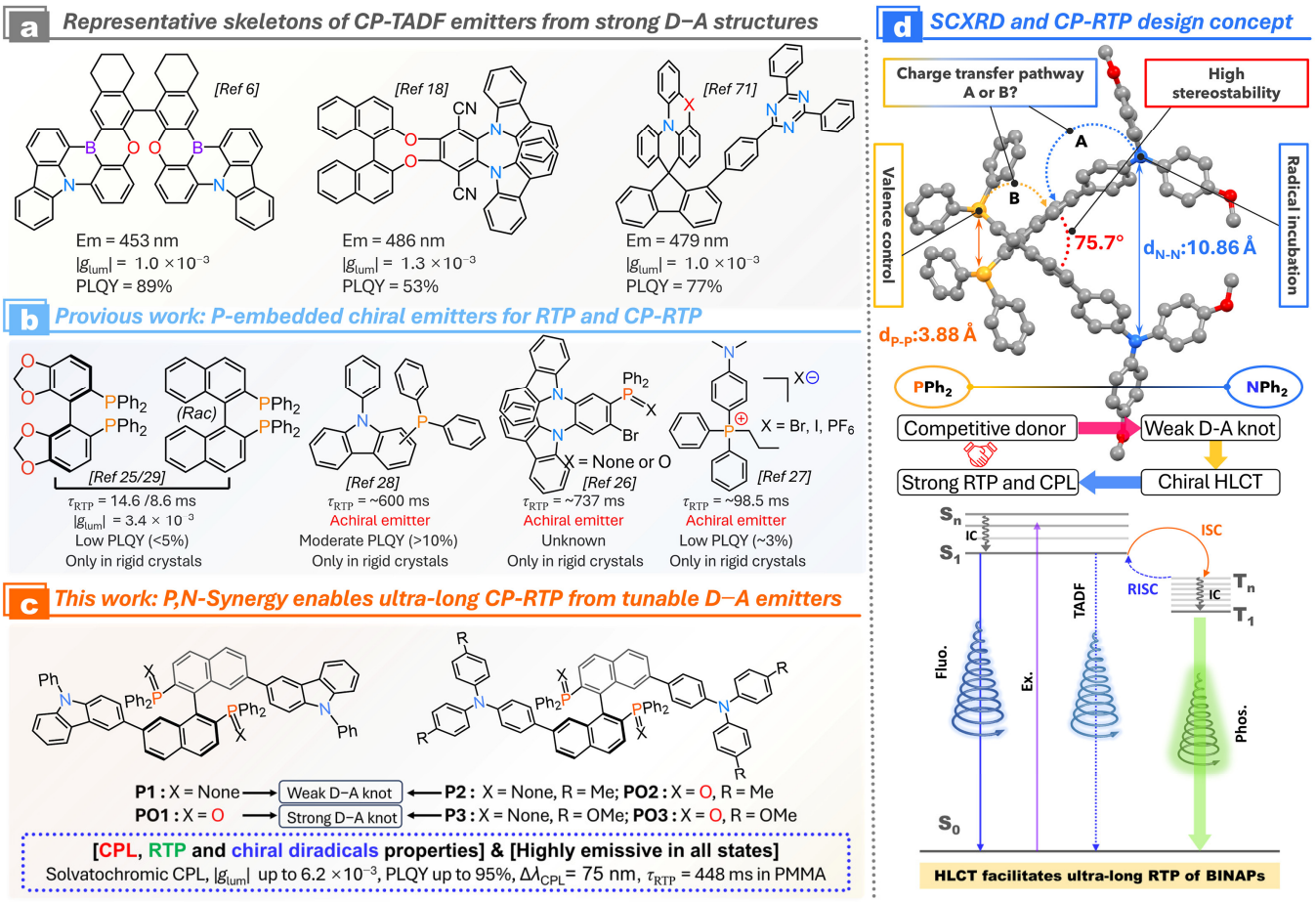


**Figure 1.** Conceptual design of single-component CPL and RTP. (a) The well-known skeleton design of chiral D–A emitters for CP-TADF. (b) P-atom embedded skeleton enables CPL or RTP. (c) Chemical structures of the CP-RTP active BINAPs based on decorative carbazole and triphenylamines. Weak D–A emitters for the integration of both CP-RTP, CP-TADF, and chiral diradicals. (d) SCXRD structure and structural characters of compound **P3** (H-atoms are omitted for clarity). Schematic illustration of a Jablonski diagram outlining the origin of possible triplet decay avenues from excited states.

luminescent performance.[29,45,46] In commercial bis(diphenylphosphino)-1,1'-binaphthyl (BINAP) ligands, the orthotropic orientation and structural motion of two naphthyl structures inhibit sufficient π–delocalization and π–π* transition, which prevent the radiation probability to emit visible light in solution.[29] We suppose that the charge transfer type could be switched from π–π* to CT via implanting the hybrid D–A moiety with huge steric hindrance (Figure 1c). The extra heteroatom insertion and rigid structure would boost the triplet local transition ($^3$LE) and $^3$CT population (*i.e.* $^3$HLCT), facilitating both RTP and CPL in any state. In view of the truth of similar valence electrons of N and P elements, the integration of electron-riched aryl phosphines and arylamines into one chiral knot would incubate weaker D–A electron separation, producing a robust HLCT and multiple SOC effects from lone-pair electrons on the N and P atoms, respectively (Figure 1d).[47,48] This characteristic HLCT might induce an effective ISC and controllable triplet decay through precisely manipulating electron-donating strength and P-atom valence state.

On the other side, the study of open-shell chiral molecules with multiple unpaired electrons on the nitrogen group elements (*e.g.* N, P, *et al*) is important for spin materials and radical catalysts.[49–52] For two unpaired electrons in one structure, diradicals might exhibit a switchable spin between high and low spin states, and thus, they are quite fascinating in chiral spintronics and optics.[53,54] Nevertheless, two unpaired single electrons in the whole system are quite reactive. In general, the delocalized resonance will cause a decreased diradical component. To improve their stability and the diradical character $y_0$, the steric protection and delocalization reinforcement are established in the previous works.[55,56] However, the chiral-associated reactivity and opto-magnetic dichroism have not been well explored on chiral ammonium and phosphonium radicals because of poor stability (including stereochemistry). Up to now, only a few chiral diradicals have been discussed by chemical oxidization, which showed small diradical characters.[55–60]

Based on the above-mentioned conception, we aim to rebuild the electronic structures of traditional BINAP ligands by creating D–A electronic knots with P and N-containing components and large steric hindrance. Herein, we introduce functional groups of N-phenylcarbazole (Cz) or triphenylamine derivatives (TPAs) into BINAP at 7,7′-positions, producing weaker D–A backbones. After facile oxidation of tervalent phosphines, the stronger pentavalent D–A emitters are facile established to enhance the CPL luminance (Figures 1c,d). These oxides display enhanced CPL brightness and chemical stability due to the tunable D–A feature. Consequently, the triplet exciton decay is highly

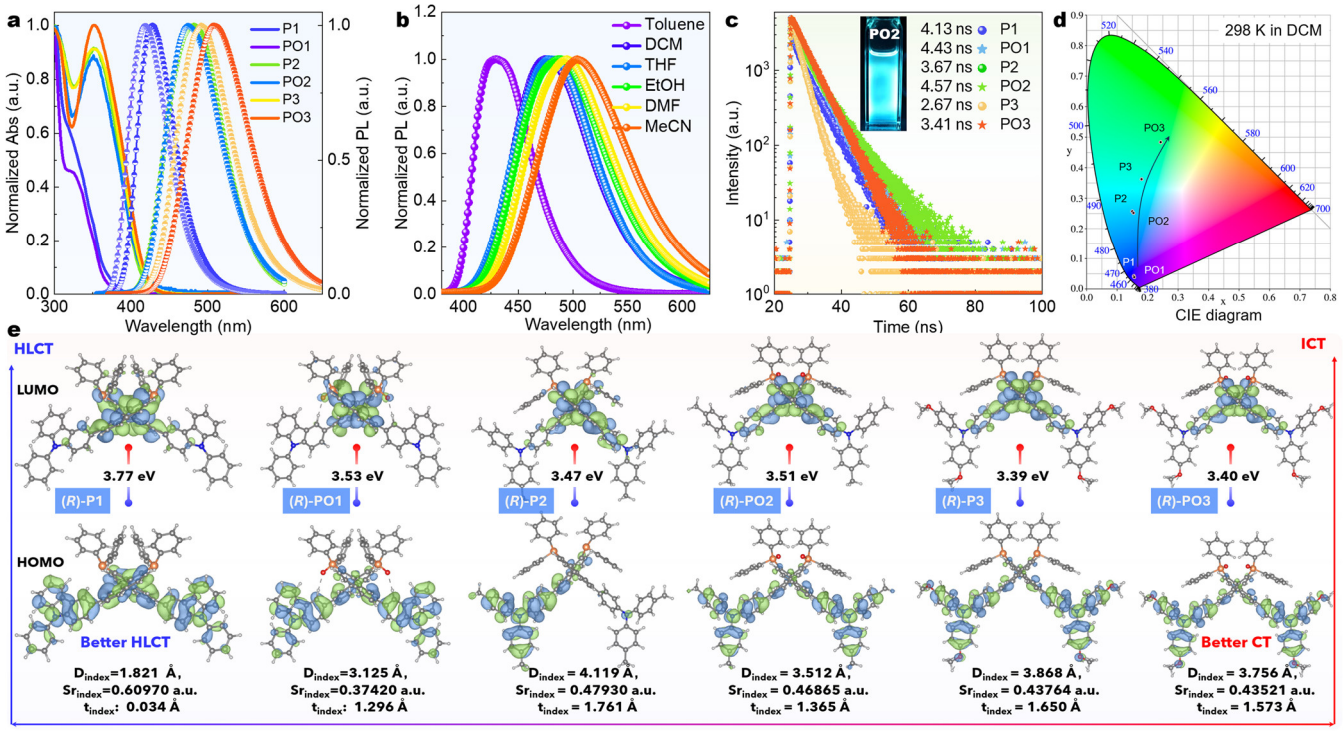


**Figure 2.** Photophysical properties and frontier molecular orbitals of emitters. (a) UV-vis and PL spectra of six emitters in DCM ($\lambda_{ex}$ = 350 nm, 298 K, $10^{-5}$ M). (b) PL spectra of **PO2** in different solvents. (c) Time-resolved emission spectra (TRPL) for their emission peaks (inserted image shows emission picture of **PO2** in DCM). (d) CIE 1931 chromaticity coordinates for six emitters in DCM. (e) HOMO and LUMO orbital distribution analysis and their calculated energy gaps of $\Delta E_{H\text{-}L}$ (*isovalue*= 0.02 a.u.).

dependent on the HLCT components, where both enhanced TPA donors and pentavalent phosphine oxide acceptors favor the CPL with a remarkable PLQY up to 95% owning to strong CT transition. However, the weak tervalent phosphine emitters exhibit ultra-long CP-RTP via key $^1$HLCT→$^3$LE authorization. In this continue, single-electron oxidation of N and P-atoms produces the chiral diradical ammoniums of phosphine oxides. Moreover, their additional diradical character and optical activity are disclosed synchronously.

## RESULTS AND DISCUSSION

The synthesis and separation of target racemic **P1**−**P3** is achieved in multiple steps according to supporting information (Figure S1).[45,61] Racemic **P1** and **P2** could be resolved into their enantiomers by HPLC on chiral stationary phase columns (>99.5% purity, >98% *ee*, Figure S2). Employing the $H_2O_2$ oxidation, highly emissive **PO1**−**PO3** emitters are obtained in equivalent yields. Their structures are confirmed by NMR, HRMS, and SCXRD (see SI). The SCXRD of ***(Rac)*-P3** reveals a $C_2$-symmetrical conformation with an axially chiral dihedral angle of 75.7° and a large N•••P distance of 9.40 Å (Figure 2a). The (*R*) and (*S*)-isomers of ***(Rac)*-P3** are packed without obvious π−π interactions due to nonplanar geometry. After the chemical oxidation of *P*-atoms, the reasonable D−A distance of N•••P atoms is established for 8.58 Å according to the density functional theory (DFT) simulation (Figure S3).

To reveal the strength of D−A nature, the photophysical properties and electronic structures of six compounds are studied by spectral measurements and DFT calculations (Figures 2b−e, Table S3). **P1**−**P3** show distinct UV-vis absorption curves from 300 to 430 nm in DCM, where the ICT bands are located at ~325 and 360 nm for **P1** and **P2**/**P3**, respectively. TPA-decorated derivatives **P2** and **P3** display enhanced CT bands because of stronger donor strength, which is in line with the oscillator strength (*f*) from time-dependent density functional theory (TD-DFT) simulation (0.177 for **P1** to 0.441 for **P3**). Compared to ligands **P1**−**P3**, their oxides **PO1**−**PO3** exhibit a slightly blue-shifted absorption but significant emission in DCM (Figure 2b). For instance, the primitive **P1** and **P2** reveal a structureless fluorescence emission at 427 and 482 nm (PLQY = 0.12, 63.1%), but **PO1** and **PO2** emit slight blue-shift light at 418 and 474 nm with boosted PLQY of 33.7 and 72.8%, respectively (Figure 2b, Table S3). Additionally, the short lifetime of emission is variated from 2.67 to 4.57 ns, indicating typical singlet-dominant fluorescence decay at room temperature for main peaks (Figure 2d). Similarly, the enhanced CT effect of methoxyls on TPAs facilitates a near-unity PLQY of 95.3% for **PO3** in degassed DCM. The emission of all oxidative emitters has obvious positive solvatochromism behaviors as well (Figure S4). As shown in Figures 2c and S15, the UV-vis spectrum of **PO2** is almost insensitive to the solvent type but the solvatochromic emission changes from 428 (toluene) to 503 nm (MeCN). The larger Stokes shifts of D−A pairs in polar solvents imply structural relaxation of polar CT excited states (Figure 2c). The stronger solvatochromic fluorescence is also observed in **P3**/**PO3** compared to **P1**, suggesting that the **P1** emission is HLCT-dominant character, while the emissive state of **P3**/**PO3** is better described as having CT feature (Figures S4, S5). The TD-DFT results of **P1** disclose the unambiguous HLCT component on electron excitation analysis, where HOMO electrons are equally located on 4-Cz and binaphthyl cores but LUMO electrons are mostly situated on binaphthyls. In addition, **P1** displays small $t_{index}$ value (0.034 Å) and hole-

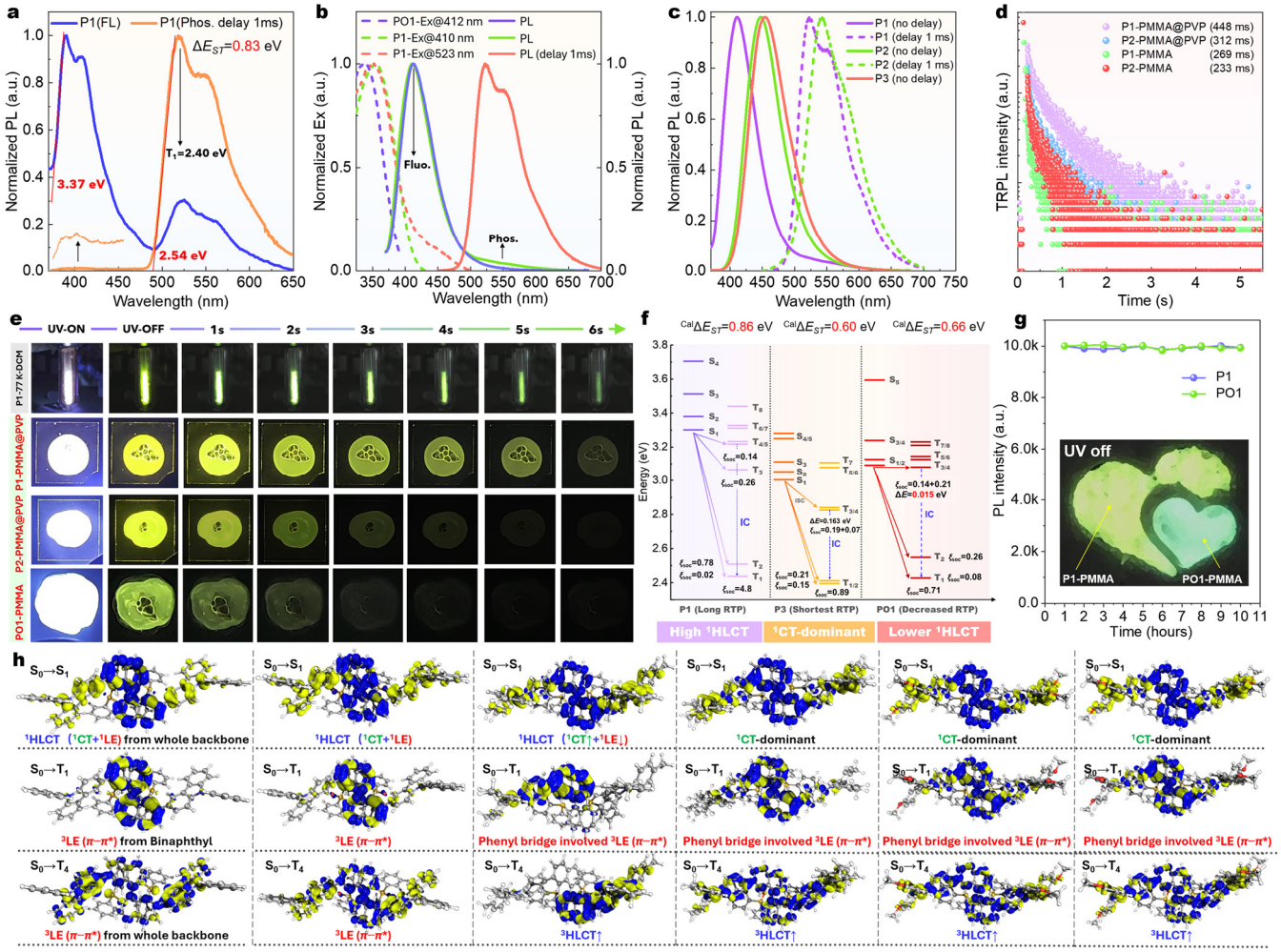


**Figure 3.** Spectroscopic and quantum-chemical investigations of phosphorescence. (a) PL and delay PL spectra of **P1** in DCM at 77 K. (b) Excitation and emission spectra of **P1** and **PO1** in PMMA@PVP films at 298 K (0.5 wt%). (c) PL and delay PL spectra of **P1–P3** in PMMA@PVP films at 298 K. (d) TRPL spectra for four doped films at their corresponding RTP peaks (lifetimes are revealed by bi-exponential fitting). (e) Representative photographs of ultra-long CP-RTP observed in the emitter doped films at ambient conditions and cryogenic DCM solutions at 77 K. (f) TD-DFT calculated energy diagrams and SOC coefficients ($\xi_{soc}$) for (***R***)**-P1**, (***R***)**-P3**, and (***R***)**-PO1** at the $S_0$ geometry. (g) PL intensity change of peak of **PO1** in PMMA with contiouns UV irradiation (inserted picture is afterglow of **P1** and **PO1** doped PMMA). (h) Electron (yellow)-hole (blue) distribution analysis of $S_0 \rightarrow S_1$ and $S_0 \rightarrow T_1/T_4$ transitions at the $S_0$ geometry (isovalue: 0.002). (*R*)-isomer are used for spectral investigations.

electron centroids distance ($D_{index}$ = 1.82 Å) but a large $S_r$ function of 0.6097 a.u. (denotes overlap of electron and hole over 60%), indicating imperfect CT in this weak D−A knot.[62–65] However, HOMO and LUMO are gradually separated as the enhanced D−A character from **P1**/**PO1** to **P3**/**PO3** (Figure 2e). These characteristics suggest that the emission originates from the ICT excited state between the TPAs and pentavalent phosphine oxide moieties (**PO2** and **PO3**), which is found to be in line with the TD-DFT calculation results and solvatochromic fluorescence (Figures 2c, S16–S18, Table S3). In consideration of the duple P/N heteroatom effects in these emitters, the phosphorescence spectra are measured in DCM at 77 K. Expectantly, the intense afterglow of **P1**−**P3** and their **PO1**−**PO3** oxides is observed at 77 K, while their low-temperature phosphorescence (LTP) lifetimes are ranged from 783 to 898 ms (Figures 3e, S11–S12). **P1** shows mixed exciton emission the 77 K (video S1), which displays two emission bands at ~400 nm ($\tau_{fluo.}$= 4.85 ns) and 518 nm with structured features (Figure 3a). The delayed LTP spectra display the same 518 nm band with long decay of 857 ms, suggesting hybrid singlet ($S_n$) and triplet ($T_n$) decay characters at cryogenic solutions. Based on the fluorescence and phosphorescence spectra onset of **P1** at 77 K, the energy gap between the lowest $S_1$ and $T_1$ excited states ($\Delta E_{S1-T1}$) is determined as large value of 0.83 eV, which is well matched to the TD−DFT simulative value (0.86 eV, Figure 3f). This nature of **P1** endows the prerequisite of organic ultra-long phosphorescence instead of TADF (Figure 3e, vide infra). Importantly, O-atom insertion not only improves PLQY for **P1**−**P3** but also the photochemical stability in solvents (Figure 3g, see last section),[25] which could benefit from the ICT effects and bonding saturation of P atoms (Table S4).[66,67]

The population and preservation of the generated triplet exciton stem from both suppressive nonradiative energy dissipation and thermal vibration relaxation.[3] Thus, **P1**−**P3** emitters are doped into polymethyl methacrylate (PMMA) or mixed PMMA@Polyvinyl pyrrolidone (PVP) polymers to enhance the molecular rigidity and isolate oxygen (details see SI). As shown in Figures 3b−d, the doped film of **P1-PMMA** emits an intense fluorescence peak at 410 nm with a short

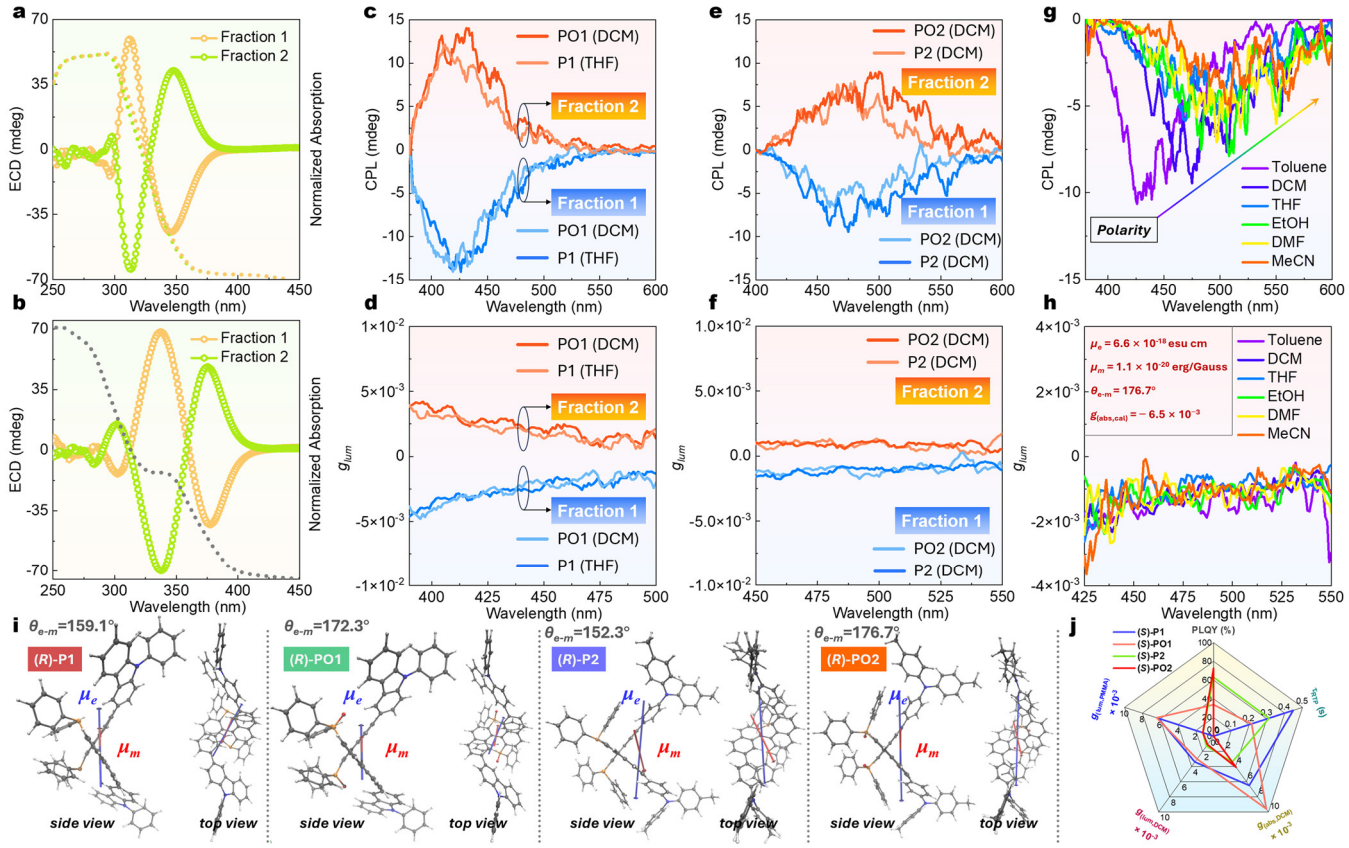


**Figure 4.** Chiral optical properties. (a–b) ECD spectra of **P1**, **P2** enantiomers in DCM ($10^{-4}$ M, fracation 1 and 2 is (*R*)-isomer and (*S*)-isomer, respectively). (c–f) CPL and $g_{lum}$ spectra of **P1**, **PO1**, **P2**, and **PO2** enantiomers in DCM ($10^{-4}$ M, $\lambda_{ex}$ = 340 nm). (g–h) Solvatochromic CPL and $g_{lum}$ spectra of **PO2** enantiomers in solvents (inserted picture shows TD-DFT simulated transition electric-magnetic dipole moments and its $\theta_{e\text{-}m}$ angle during $S_0 \rightarrow S_1$ transition for **(*R*)-PO2**). (i) Calculated electric (blue arrow, $\mu_e$) and magnetic (red arrow, $\mu_m$) transition dipole moments at the B3LYP-D3/6-31G(d) level for $S_0 \rightarrow S_1$. (j) Chiroptical properties comparison of four emitters in this work.

decay of 8.58 ns and a tail at 523 nm with an ultra-long decay of $\tau_{avg}$ = 269 ms (Figures 3d, S14a). Moreover, this RTP band overlaps well with their LTP spectra (~520 nm), demonstrating the same decay channel from monomers. After further optimization of the polymer matrix, the **P1-PMMA@PVP** film displays a similar phosphorescence band but an extended lifetime of 448 ms, which could be related to the elevated rigidity of the polymer frameworks (Figures 3d–e, S7, videos S2–S3).[44] Similarly, the RTP with a faster decay has been observed in **PO1** and **P2** doped polymers, and their RTP lifetimes are gradually decreased to 233 and 218 ms, respectively (Figure 3c, Table S3). This tendency is supported by the additional O-atoms incorporation from methoxyl and P=O units in **PO2**, **P3**, and **PO3**, where the fluorescent quantum efficiency is boosted but weak afterglow is indistinguishable by naked eyes observation (Figures S8, S9, Table S3, video S4). With the high-resolutive phosphorescence test with a short time-gate of 0.1 ms, the weak RTP is recorded (Figure S6b). Time-resolved photoluminescence (TRPL) spectra reveal the short RTP lifetimes of a millisecond regime (Figures S14f, S14g). Their afterglow is significantly shorter than that of the **P1**-doped polymer, indicating a fast triplet decay speed of CT-driven emitters. This phenomenon has also been noticed in donor-fused Corannulenes by a recent Zysman-Colman's work.[24]

TD–DFT simulative results have been analyzed to elucidate the phosphorescence decay mechanism. For the $S_0 \rightarrow S_1$ transition of emitter **P1**, the $^1$LE transition is driven by $^1\pi$–$\pi^*$ in binaphthyl itself, and the weak $^1$CT originates from the Cz donors and binaphthyl acceptor (Figures 2e, 3h). The lone pair *p*-electrons of N-atoms have a prominent HOMO occupation and transfer via the $^1$CT channel during the $S_0 \rightarrow S_1$ (H–L = 95.1%, $f$ = 0.177) transition (Table S5), suggesting the $^1$HLCT behavior. Furthermore, the hole-electron analysis documents of $T_1$ and $T_2$ states have an exclusive $^3$LE character rather than $^3$CT, in which the hole-electron pairs are overlayed on the binaphthyl (Figures 3h, S20). In contrast, the higher $T_3$/$T_4$/$T_5$ states have dispersive $^3$LE ($^3$n–$\pi^*$ and $^3\pi$–$\pi^*$) transition on both binaphthyl and Cz units to promote the spin-flipping from HLCT-type $S_1$, following El-Sayed's rule.[3,23] In this condition, TD-DFT profiles reveal a small spin-orbit coupling coefficient of $S_1$–$T_1$ ($\xi_{soc}\{S_1\text{–}T_1\}$ = 0.02 cm$^{-1}$) but larger magnitudes of $S_1$–$T_{2\text{-}5}$ (0.14 to 0.78 cm$^{-1}$) and $S_0$–$T_1$ (4.8 cm$^{-1}$) (Figures 3f, S20). According to those above-discussed identifications and matched experimental energy gaps and emission energy ($^{exp}\Delta E_{S1\text{–}T1}$ = 0. 83 eV, $^{exp}E_{T1}$ = 2.40 eV, $^{cal}E_{T1}$ = 2.44 eV) in **P1**, it is concluded that the RTP is originated from lowest $T_1$ state via effective ISC in $S_1 \rightarrow T_{2\text{-}5}$ and sufficient internal conversion (IC) between $T_{2\text{-}5}$ and $T_1$. In a sharp contrast to **P1**, the calculated results of **P3** clarify a perfect singlet $^1$CT (from TPAs to binaphthyl) process instead of $^1$HLCT of $S_0 \rightarrow S_1$, while the delocalization-reinforced $^3$LE of $S_0 \rightarrow T_{1\text{-}4}$ is documented on phenyl bridges. Thus, the electron-hole separation enables a smaller $\Delta E_{S1\text{–}T1}$ value of 0.60 eV. The degenerated $\Delta E_{S1\text{–}T3/4}$ shows a modest $\xi_{soc}$ addition of 0.26

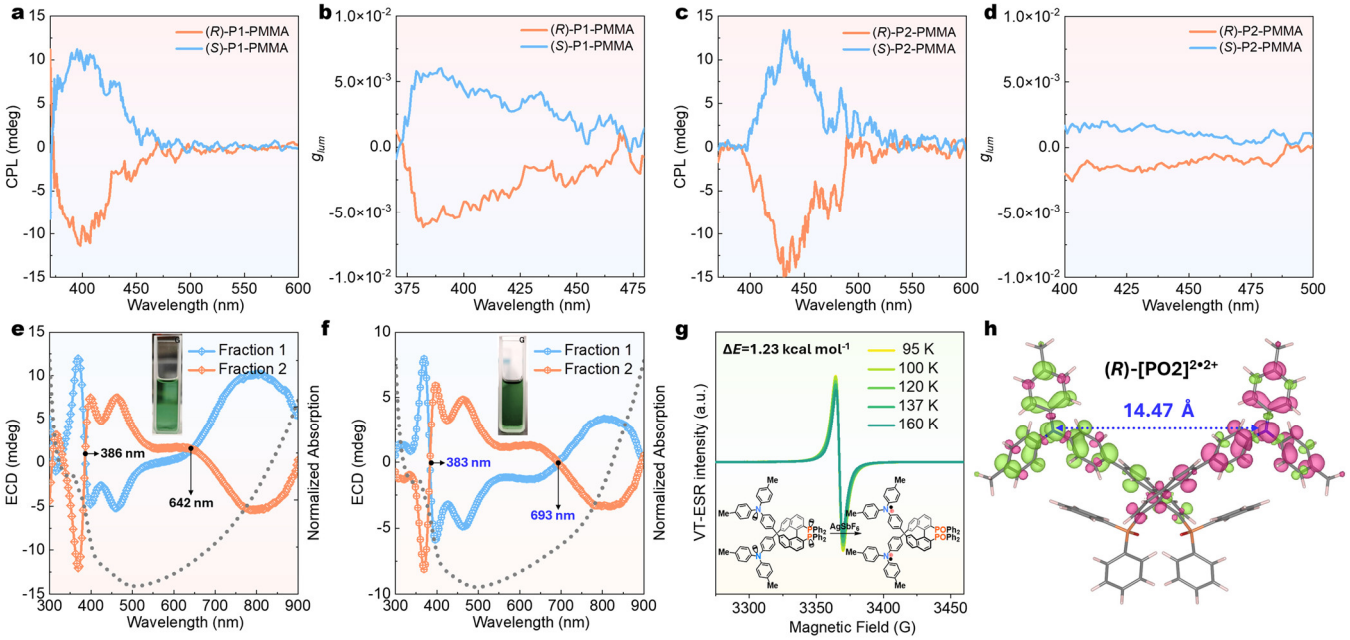


**Figure 5.** CPL and chiroptical activity of P1−P2 and $[PO2]^{2\bullet 2+}[(SbF_6)_2]^{2-}$, respectively. (a–d) CPL and $g_{lum}$ spectra of **P1** and **P2** enantiomers in doped PMMA (0.5 wt%). (e–f) ECD spectra and solution photographs of $\mathbf{[P2]^{2\bullet 2+}[(SbF_6)_2]^{2-}}$ and $\mathbf{[PO2]^{2\bullet 2+}[(SbF_6)_2]^{2-}}$ enantiomers in DCM at ambient conditions. (g) VT-ESR spectra of $\mathbf{[PO2]^{2\bullet 2+}[(SbF_6)_2]^{2-}}$ in dry DCM. (h) Spin density population of $\mathbf{(\textit{R})\text{-}[PO2]^{2\bullet 2+}}$ at UB3LYP−D3/6−31G(d) level.

$cm^{-1}$ and an energy gap of 0.16 eV, which allow a fast ISC by the $^1$CT→$^3$LE ($S_1$−$T_1$) transition. The subsequent IC follows $^3$HLCT to $^3\pi$–$\pi$* progress (Figures 3, S9, S25, video S4). These outcomes imply a crucial HLCT-governing triplet decay for ultra-long RTP emission from weak D−A structures. Overall, for the continuous reinforcement of D−A competence, every sample follows the progressive alteration of electron transition from $^1$HLCT ($S_1$) to $^1$CT ($S_1$) as well as $^3$LE ($T_1$) to $^3$HLCT ($T_1$) (Figures 3h, S20−S25), which might cause the discrepant inheritance of spin state between $^3$HLCT ($T_4$) and $^3$LE ($^3\pi$–$\pi$*, $T_1$) via IC. Noteworthy, the emitters carry different donor substituents but show similar phosphorescence bands (Figures 3c), indicating that triplet decay should be derived from the common binaphthyl core.[29] This hypothesis is also substantiated by the $^3$LE occupy of binaphthyl. Thus, the existence of the $^3\pi$–$\pi$* ($T_1$) triplet is essential for the long-lived RTP. The shoulder of the RTP band is produced by the vibronic coupling of the triplet, where the triplet excited state communication is present in the D−A unit via HLCT.[25,33,45] As a consequence, the synergetic incorporation of n–$\pi$* from lone-pair electrons on P and N atoms as well as HLCT states from weak D−A electronic structures would facile regulate the ISC and IC process, endowing the desired ultra-long RTP. However, the immoderate reinforcement of D−A specialty will accelerate the triplet decay rate via CT dominance,[24,26,28] bringing higher fluorescence PLQY but short lifetimes of CP-RTP (Figure 3g). Using different decay times and flexible manufacturing potential of doped films for **P1**−**P2**, the distinct afterglow films have been prepared by the drop-casting method (Figure 3e). Under the 365 nm light, the films document a strong blue emission. After removing the UV flashlight, the sequential yellow-green afterglow could be observed by the naked eyes for a long time, up to 10 seconds for **P1-PMMA@PVP** (videos S2−S4). In addition, this flexible film could be curled and used under moist conditions for practical applications in optical encryption (Figure S26).

To evaluate the P,N-synergy triggered chiroptical performance of **P1**−**P2** and **PO1**−**PO2** enantiomers. Electronic circular dichroism (ECD) and CPL spectra are collected in different solvents. At first, the stereo-conformation for chiral-HPLC separated isomers is determined by comparing both experimental ECD and CPL spectra with the ones calculated by the TD−DFT results (Figure S28). The first fraction of chiral HPCL belongs to the (*R*)-isomer and the second is the (*S*)-isomer. Similar to solvent-insensitive UV-vis absorption, all ECD curves are almost identical in variational solvents from toluene to MeCN (Figures S15a−S15b). In DCM, the trivalent phosphines **(*R*)/(*S*)-P1** and **(*R*)/(*S*)-P2** exhibit a similar ECD curve shape from 250−450 nm except for red-shifted absorption and exciton split spots (Figures 4a,b). The oxides of **PO1** and **PO2** have slightly hypochromatic CD signals and higher absorption dissymmetry factors ($g_{abs}$, Table S4). These $g_{abs}$ values manifest a maximum at the lowest-energy CT absorption band, with a range of 3.4 to 9.6 × $10^{-3}$ in all investigated compounds for (*S*)-configuration (Table S3), suggesting effective chiral induction and expression in this axially chiral D−A skeleton. The oxides have slightly larger $g_{abs}$ values, which are mainly caused by larger electric-magnetic dipole moment angles (Figures 5i, S28−S30). Remarkably, the stereochemic robustness of **(*R*)-PO1** and **(*R*)-PO2** are elucidated according to chiral conformation analysis by variable temperature ECD spectra. The ECD spectra of compounds are unchanged after 180 °C heating for 3 hours, unmasking ultrahigh stereo conformation stability by virtue of the robust hindrance (Figure S29).

The optical activity of excited states for enantiomeric **P1**, **P2**, **PO1**, and **PO2** was elucidated through CPL spectroscopy (Figures 4c−f, 4j), revealing strong CPL with the large luminescence dissymmetry factors ($g_{lum}$) ranging from ~3.4 × $10^{-3}$ (**P1**) to 1.3 × $10^{-3}$ (**P2**) in DCM, which are comparable to other best emissive TADF emitters.[18,39,68–71] However, the excellent stereo conformation stability and solvatochromic

CPL represent state-of-the-art performance.[18] TD-DFT calculations provide further physical insights into the ECD absorption and excitation-emission processes of the ground ($S_0$) and excited states ($S_1$). For **(*R*)-P1**, the $S_0 \rightarrow S_1$ processes balanced electron transition dipole moment ($\mu_e = 3.76 \times 10^{-18}$ esu cm), magnetic transition dipole moment ($\mu_m$ = 8.05 × $10^{-21}$ erg/Gauss), large $\mu_e$–$\mu_m$ angle ($\theta_{e\text{-}m}$ = 159.1°), and $g_{(abs,cal)}$ of $-8.0 \times 10^{-3}$, which are in agreement with experimental results $g_{(abs,exp)} = -6.5 \times 10^{-3}$, Figures S28, S30). Other compounds exhibit approximate $g_{(abs,cal)}$ levels for $S_0 \rightarrow S_1$ transition (Figures S21, S32–S35). In this case, the $S_1 \rightarrow S_0$ of **(*R*)-P1** could inherit these equivalent transition conditions ($\theta_{e\text{-}m}$ = 163.6°), which produces both robust $g_{(lum,exp)} = 6.2 \times 10^{-3}$ and $g_{(lum,cal)} = 7.0 \times 10^{-3}$ for CPL in rigid polymers (Figures 5a–b, S32, S37).

Importantly, the solvatochromic CPL has also been explored for enantiomeric **PO1** and **PO2** emitters (Figures 4g–h, S31). In the polar solvents, the CPL becomes broad emission and large Stokes shifts because the structural reorganization occurs during the excitation-emission progress. The case in point is **(*R*)/(*S*)-PO1** emits deep-blue CPL with negative and positive signals at 416 nm in nonpolar toluene but 440 nm in polar MeCN ($\Delta\lambda_{max}$ = ~25 nm). Their $g_{lum}$ has reached maximums of $\pm 5.0 \times 10^{-3}$ in toluene. In comparison to **(*R*)/(*S*)-PO1**, **(*R*)/(*S*)-PO2** have a stronger D–A character, endowing a more significant solvatochromic CPL wavelength change of $\Delta\lambda_{max}$ = 75 nm, which is among the highest values for chiral D–A molecules.[67,72] Noteworthy, the CPL performance of doped PMMA films displays an equivalent $|g_{lum}|$ level (~1.2 to 6.2 × $10^{-3}$) in contrast to the solutions but reserves high PLQY and ultra-long RTP due to suppressive structural relaxation (Figures 5a–d, S31, S36–S37). From a comparison perspective, in the pace of CT enhancement and high PLQY, the *g* values and RTP lifetimes suffer deterioration. Thus, **PO1** holds balanced quantum efficiency and ultra-long CP-RTP in all samples (Figure 4j).

In this work, via the implantation of nonplanar chiral backbones and D–A moieties, we build sufficiently stable diradicals with chiral genes. As shown in Figure 5f, the neutral **(*S*)-PO2** could be transformed into a diradical ammonium **[(*S*)-PO2]$^{2\bullet 2+}$[(SbF$_6$)$_2$]$^{2-}$** by adding excess chemical oxidant of $AgSbF_6$ (Figure S38a). **(*S*)-PO2** in DCM is colorless under daylight but it changes into green after chemical oxidation. UV–vis–IR absorption of the **[(*S*)-PO2]$^{2\bullet 2+}$[(SbF$_6$)$_2$]$^{2-}$** solution exhibits a new absorption onset at around 1100 nm and vibronic visible signatures (Figure S38e). Using the same condition, **(*Rac*)-PO3** is quantitatively converted to **[(*Rac*)-PO3]$^{2\bullet 2+}$[(SbF$_6$)$_2$]$^{2-}$**, which shows similar UV–vis–IR absorption efficacy to **[(*S*)-PO2]$^{2\bullet 2+}$[(SbF$_6$)$_2$]$^{2-}$** with half-life evaluation to be ~6 days via electron spin resonance (ESR) monitoring in atmosphere conditions (Figure S39). These results imply a remarkable persistence for those above radical species. Unambiguously, ESR analysis of radical products reveals the presence of diradial characters. Specifically, the ESR of **[(*S*)-PO2]$^{2\bullet 2+}$[(SbF$_6$)$_2$]$^{2-}$** exhibits a broad but intensive signal in the $|\Delta m_s| = 1$ region. The half-field $|\Delta m_s| = 2$ region also manifests a characteristic signal, which strongly supports a diradicals affiliation (Figures S38b–S38d).[32,45] The broad and weak ESR split also suggests weak interactions between two radical ammoniums. Spin-unrestricted DFT calculation of **[(*S*)-PO2]$^{2\bullet 2+}$** dication at UB3LYP–D3/6–31G(d) level shows a large N•••N distance ($d_{N\text{-}N}$ = 14.47 Å) since coulombic repulsion of ammoniums. Spin density population is partly delocalized on two TPAs and binaphthyl units to increase the stability (Figure 5h). The diradical character $y_0$ of **[(*S*)-PO2]$^{2\bullet 2+}$** is calculated to be 0.953 by Yamaguchi's scheme at the same UB3LYP–D3/6–31G(d) level (details see SI), which surpasses the previous TPA-based chiral diradicals ($y_0$ = 0.53, 0.64).[56,73] Besides, the VT-ESR experiment is executed to unveil the spin ground state in **[(*S*)-PO2]$^{2\bullet 2+}$[(SbF$_6$)$_2$]$^{2-}$**. The IT intensities gradually decrease with decreasing temperature from 160 to 95 K, corroborating a singlet ground state of these diradicals (Figure 5g). The Bleaney–Bowers equation fitting gives a small singlet-triplet energy gap ($\Delta E_{S-T}$ = −1.23 kcal mol$^{-1}$) of diradicals.[56,74] Expectant diradicals with chiral triplet ground state and strong coupling effects are still in progress in our lab. Benefiting from good chemical and stereoscopic conformation stability of **[(*S*)/(*R*)-PO2]$^{2\bullet 2+}$[(SbF$_6$)$_2$]$^{2-}$**, their chiral optical properties have been disclosed by ECD measurements, which show remarkable circularly polarized light absorption in the NIR region, as indicated by its absorption anisotropy factor, $|g_{abs}| = 2.6 \times 10^{-4}$ at 920 nm (Figure 5f). On the other hand, the trivalent phosphine of **(*S*)/(*R*)-P1** is chemically unstable in the presence of $AgSbF_6$, which could be gradually transformed into **[(*S*)/(*R*)-PO2]$^{2\bullet 2+}$[(SbF$_6$)$_2$]$^{2-}$** in air. The *in situ* ECD monitoring of oxidation for **(*S*)/(*R*)-P1** system displays a very similar ECD trace compared to **[(*S*)/(*R*)-PO2]$^{2\bullet 2+}$[(SbF$_6$)$_2$]$^{2-}$** (Figures 5e,f), implying mixed species of radicals from mono oxidation and ultimate dioxidation of two P-atoms (Figure S42).

In fact, the single-electron transfer process of P-atom is quite different by chemical oxidation and photoinduced electron transfer (PET) of phosphines at ambient conditions.[25,45,46] This feature is mainly related to the oxytropic predilection and chelation of P-atom. Under air conditions with continuous UV light irradiation, **P1** is a photodegradable skeleton in solution. The new broad PL band is observed with a peak at ~613 nm, where the color of emission is changed from blue to pink (Figures S43b, S43e). Spectral and HRMS detection data manifest a cyclization product from phosphonium radical species (Figures S43a-i).[75] Recent research has uncovered that this molecular restructuring is a common feature of photochromic phosphines.[25,45,46] On the contrary, **P1** is still stable in protecting PMMA (Figure 3g).

## Discussion

In summary, we have firstly validated the general concept for designing ultra-long CP-RTP and stable chiral diradicals via synchronous implantation of HLCT in P,N-doping BINAPs. These tunable D–A emitters not only endow controllable HLCT excited states to optimize the intersystem crossing but also the chiral environment, facilitating the solvatochromic CPL and ultra-long CP-RTP. Their triplet decay speed and channel highly depend on the ICT strength, which could be adjusted by altering the donors, together with associated variable valency on the P-atom. Moreover, the TPA diradicals are isolated by a chiral binaphthalene bridge, which endows the high diradical character and NIR optical activity because of high structural stability. Given the diversity of BNIAPs and other phosphine ligand skeletons, we believe this P,N-synergetic strategy would provide new candidates for the development of efficient CPL emitters, and chiral-driven spin materials from chiral phosphines and their oxides.

## Accession codes

CCDC number 2344550 contains the supplementary crystallographic data for this paper. These data can be obtained free of charge via www.ccdc.cam.ac.uk/data_request/cif, or by emailing data_request@ccdc.cam.ac.uk, or by contacting The Cambridge Crystallographic Data Centre, 12 Union Road, Cambridge CB2 1EZ, UK; fax: +44 1223 336033.

## Data availability statement

The data that support the findings of this study are available from ESI or the corresponding author upon reasonable request.

## Conflict of interest

The authors declare no conflict of interest.

## Acknowledgements

This research was supported by the National Natural Science Foundation of China (No. 21871133), the Natural Science Foundation of Jiangsu Province (No. BK20211146), and the Science, Technology, and Innovation Commission of Shenzhen Municipality (No. JCYJ20180307153251975) for financial support.

## Author contributions

W. H. supervised the project and revised the manuscript. B. Y. conducted the research design, property studies, and paper preparation. All authors discussed the research results and contributed to the paper.

## References

(1) Chen, B.; Huang, W.; Zhang, G. Observation of Chiral-Selective Room-Temperature Phosphorescence Enhancement via Chirality-Dependent Energy Transfer. *Nat. Commun.* **2023**, *14*, 1514.

(2) Zhang, G.; Palmer, G. M.; Dewhirst, M. W.; Fraser, C. L. A Dual-Emissive-Materials Design Concept Enables Tumour Hypoxia Imaging. *Nat. Mater.* **2009**, *8*, 747–751.

(3) Zhao, W.; He, Z.; Tang, B. Z. Room-Temperature Phosphorescence from Organic Aggregates. *Nat. Rev. Mater.* **2020**, *5*, 869–885.

(4) Hirata, S.; Vacha, M. Circularly Polarized Persistent Room-Temperature Phosphorescence from Metal-Free Chiral Aromatics in Air. *J. Phys. Chem. Lett.* **2016**, *7*, 1539–1545.

(5) Zhang, D. W.; Li, M.; Chen, C. F. Axially Chiral Materials Exhibiting Blue-Emissive Ultralong Organic Phosphorescence and Intense Circularly Polarized Luminescence. *Sci. China Mater.* **2023**, *66*, 4030–4036.

(6) Yan, Z. P.; Yuan, L.; Zhang, Y.; Mao, M. X.; Liao, X. J.; Ni, H. X.; Wang, Z. H.; An, Z.; Zheng, Y. X.; Zuo, J. L. A Chiral Dual-Core Organoboron Structure Realizes Dual-Channel Enhanced Ultrapure Blue Emission and Highly Efficient Circularly Polarized Electroluminescence. *Adv. Mater.* **2022**, *34*, 2204253.

(7) Huang, Z.; He, Z.; Ding, B.; Tian, H.; Ma, X. Photoprogrammable Circularly Polarized Phosphorescence Switching of Chiral Helical Polyacetylene Thin Films. *Nat. Commun.* **2022**, *13*, 7841.

(8) Zhang, M.; Guo, Q.; Li, Z.; Zhou, Y.; Zhao, S.; Tong, Z.; Wang, Y.; Li, G.; Jin, S.; Zhu, M.; Zhuang, T.; Yu, S. H. Processable Circularly Polarized Luminescence Material Enables Flexible Stereoscopic 3D Imaging. *Sci. Adv.* **2023**, *9*, eadi9944.

(9) Li, H.; Gu, J.; Wang, Z.; Wang, J.; He, F.; Li, P.; Tao, Y.; Li, H.; Xie, G.; Huang, W.; Zheng, C.; Chen, R. Single-Component Color-Tunable Circularly Polarized Organic Afterglow through Chiral Clusterization. *Nat. Commun.* **2022**, *13*, 429.

(10) Xu, S.; Chen, R.; Zheng, C.; Huang, W. Excited State Modulation for Organic Afterglow: Materials and Applications. *Adv. Mater.* **2016**, *28*, 9920–9940.

(11) Li, Y.; Gecevicius, M.; Qiu, J. Long Persistent Phosphors - From Fundamentals to Applications. *Chem. Soc. Rev.* **2016**, *45*, 2090–2136.

(12) Rodríguez, R.; Naranjo, C.; Kumar, A.; Matozzo, P.; Das, T. K.; Zhu, Q.; Vanthuyne, N.; Gómez, R.; Naaman, R.; Sánchez, L.; Crassous, J. Mutual Monomer Orientation to Bias the Supramolecular Polymerization of [6]Helicenes and the Resulting Circularly Polarized Light and Spin Filtering Properties. *J. Am. Chem. Soc.* **2022**, *144*, 7709–7719.

(13) Romero, N. A.; Nicewicz, D. A. Organic Photoredox Catalysis. *Chem. Rev.* **2016**, *116*, 10075–10166.

(14) Gu, L.; Ye, W.; Liang, X.; Lv, A.; Ma, H.; Singh, M.; Jia, W.; Shen, Z.; Guo, Y.; Gao, Y.; Chen, H.; Wang, D.; Wu, Y.; Liu, J.; Wang, H.; Zheng, Y. X.; An, Z.; Huang, W.; Zhao, Y. Circularly Polarized Organic Room Temperature Phosphorescence from Amorphous Copolymers. *J. Am. Chem. Soc.* **2021**, *143*, 18527–18535.

(15) Zhang, D. W.; Li, M.; Chen, C. F. Recent Advances in Circularly Polarized Electroluminescence Based on Organic Light-Emitting Diodes. *Chem. Soc. Rev.* **2020**, *49*, 1331–1343.

(16) Yang, J.; Fang, M.; Li, Z. Stimulus-Responsive Room Temperature Phosphorescence Materials: Internal Mechanism, Design Strategy, and Potential Application. *Accounts Mater. Res.* **2021**, *2*, 644–654.

(17) Sun, S.; Li, X.; Xu, C.; Li, Y.; Wu, Y.; Feringa, B. L.; Tian, H.; Ma, X. Scale Effect of Circularly Polarized Luminescent Signal of Matter. *Natl. Sci. Rev.* **2023**, *10*, nwad072.

(18) Feuillastre, S.; Pauton, M.; Gao, L.; Desmarchelier, A.; Riives, A. J.; Prim, D.; Tondelier, D.; Geffroy, B.; Muller, G.; Clavier, G.; Pieters, G. Design and Synthesis of New Circularly Polarized Thermally Activated Delayed Fluorescence Emitters. *J. Am. Chem. Soc.* **2016**, *138*, 3990–3993.

(19) Uoyama, H.; Goushi, K.; Shizu, K.; Nomura, H.; Adachi, C. Highly Efficient Organic Light-Emitting Diodes from Delayed Fluorescence. *Nature* **2012**, *492*, 234–238.

(20) Zhang, Q.; Li, J.; Shizu, K.; Huang, S.; Hirata, S.; Miyazaki, H.; Adachi, C. Design of Efficient Thermally Activated Delayed Fluorescence Materials for Pure Blue Organic Light Emitting Diodes. *J. Am. Chem. Soc.* **2012**, *134*, 14706–14709.

(21) Wong, M. Y.; Zysman-Colman, E. Purely Organic Thermally Activated Delayed Fluorescence Materials for Organic Light-Emitting Diodes. *Adv. Mater.* **2017**, *29*, 1605444.

(22) Tao, Y.; Yuan, K.; Chen, T.; Xu, P.; Li, H.; Chen, R.; Zheng, C.; Zhang, L.; Huang, W. Thermally Activated Delayed Fluorescence Materials Towards the Breakthrough of Organoelectronics. *Adv. Mater.* **2014**, *26*, 7931–7958.

(23) Wang, T.; Gupta, A. K.; Wu, S.; Slawin, A. M. Z.; Zysman-Colman, E. Conjugation-Modulated Excitonic Coupling Brightens Multiple Triplet Excited States. *J. Am. Chem. Soc.* **2023**, *145*, 1945–1954.

(24) Si, C.; Wang, T.; Gupta, A. K.; Cordes, D. B.; Slawin, A. M. Z.; Siegel, J. S.; Zysman-Colman, E. Room-Temperature Multiple Phosphorescence from Functionalized Corannulenes: Temperature Sensing and Afterglow Organic Light-Emitting Diode**. *Angew. Chem. Int. Ed.* **2023**, *62*, e202309718.

(25) Yang, B.; Yan, S.; Zhang, Y.; Ban, S.; Ma, H.; Feng, F.; Huang, W. Double-Model Decay Strategy Integrating Persistent Photogenic Radicaloids with Dynamic Circularly Polarized Doublet Radiance and Triplet Afterglow. *J. Am. Chem. Soc.* **2024**, *146*, 7668−7678.

(26) Lu, G.; Tan, J.; Wang, H.; Man, Y.; Chen, S.; Zhang, J.; Duan, C.; Han, C.; Xu, H. Delayed Room Temperature Phosphorescence Enabled by Phosphines. *Nat. Commun.* **2024**, *15*, 3705.

(27) Alam, P.; Cheung, T. S.; Leung, N. L. C.; Zhang, J.; Guo, J.; Du, L.; Kwok, R. T. K.; Lam, J. W. Y.; Zeng, Z.; Phillips, D. L.; Sung, H. H. Y.; Williams, I. D.; Tang, B. Z. Organic Long-Persistent Luminescence from a Single-Component Aggregate. *J. Am. Chem. Soc.* **2022**, *144*, 3050–3062.

(28) Song, X.; Lu, G.; Man, Y.; Zhang, J.; Chen, S.; Han, C.; Xu, H. Phosphine-Manipulated p-π and π-π Synergy Enables Efficient Ultralong Organic Room-Temperature Phosphorescence. *Angew. Chem. Int. Ed.* **2023**, *62*, e202300980.

(29) Wu, X.; Huang, C. Y.; Chen, D. G.; Liu, D.; Wu, C.; Chou, K. J.; Zhang, B.; Wang, Y.; Liu, Y.; Li, E. Y.; Zhu, W.; Chou, P. T. Exploiting Racemism Enhanced Organic Room-Temperature Phosphorescence to Demonstrate Wallach's Rule in the Lighting Chiral Chromophores. *Nat. Commun.* **2020**, *11*, 2145.

(30) Tang, M.-C.; Chan, M.-Y.; Yam, V. W.-W. Molecular Design of Luminescent Gold(III) Emitters as Thermally Evaporable and Solution-Processable Organic Light-Emitting Device (OLED) Materials. *Chem. Rev.* **2021**, *121*, 7249–7279.

(31) Li, T.-Y.; Zheng, S.-J.; Djurovich, P. I.; Thompson, M. E. Two-Coordinate Thermally Activated Delayed Fluorescence Coinage Metal Complexes: Molecular Design, Photophysical Characters, and Device Application. *Chem. Rev.* **2024**, *124*, 4332–4392.

(32) Yam, V. W.-W.; Au, V. K.-M.; Leung, S. Y.-L. Light-Emitting Self-Assembled Materials Based on D8 and D10 Transition Metal Complexes. *Chem. Rev.* **2015**, *115*, 7589–7728.

(33) Sumsalee, P.; Abella, L.; Roisnel, T.; Lebrequier, S.; Pieters, G.; Autschbach, J.; Crassous, J.; Favereau, L. Axial and Helical Thermally Activated Delayed Fluorescence Bicarbazole Emitters: Opposite Modulation of Circularly Polarized Luminescence through Intramolecular Charge-Transfer Dynamics. *J. Mater. Chem. C* **2021**, *9*, 11905–11914.

(34) Deng, M.; Mukthar, N. F. M.; Schley, N. D.; Ung, G. Yellow Circularly Polarized Luminescence from C1-Symmetrical Copper(I) Complexes. *Angew. Chem. Int. Ed.* **2020**, *59*, 1228–1231.

(35) Muthig, A. M. T.; Mrózek, O.; Ferschke, T.; Rödel, M.; Ewald, B.; Kuhnt, J.; Lenczyk, C.; Pflaum, J.; Steffen, A. Mechano-Stimulus and Environment-Dependent Circularly Polarized TADF in Chiral Copper(I) Complexes and Their Application in OLEDs. *J. Am. Chem. Soc.* **2023**, *145*, 4438–4449.

(36) Chen, L.; Li, C.; Liu, Z. F.; Kuboi, Y.; Fu, E.; Vargas, L. S.; Adachi, C.; Mathevet, F.; Zhang, S. A Donor-Acceptor Cage for Circularly Polarized TADF Emission. *Chem. Commun.* **2024**, *60*, 1758–1761.

(37) Xu, Y.; Hafeez, H.; Seibert, J.; Wu, S.; Ortiz, J. S. O.; Crassous, J.; Bräse, S.; Samuel, I. D. W.; Zysman-Colman, E. [2.2]Paracyclophane-Substituted Chiral Multiresonant Thermally Activated Delayed Fluorescence Emitters for Efficient Organic Light-Emitting Diodes. *Adv. Funct. Mater.* **2024**, 2402036.

(38) He, B.; Zhong, Q.; Dong, Q.; Yang, X.; Cowling, S. J.; Qiao, W.; Bruce, D. W.; Zhu, W.; Duan, P.; Wang, Y. Liquid-Crystalline Circularly Polarised

TADF Emitters for High-Efficiency, Solution-Processable Organic Light-Emitting Diodes. *Mater. Horizons* **2023**, *11*, 1251–1260.
(39) Meng, G.; Zhou, J.; Han, X. S.; Zhao, W.; Zhang, Y.; Li, M.; Chen, C. F.; Zhang, D.; Duan, L. B-N Covalent Bond Embedded Double Hetero-[n]Helicenes for Pure Red Narrowband Circularly Polarized Electroluminescence with High Efficiency and Stability. *Adv. Mater.* **2024**, *36*, 2307420.
(40) Zhao, W.; He, Z.; Lam, J. W. Y.; Peng, Q.; Ma, H.; Shuai, Z.; Bai, G.; Hao, J.; Tang, B. Z. Rational Molecular Design for Achieving Persistent and Efficient Pure Organic Room-Temperature Phosphorescence. *Chem* **2016**, *1*, 592–602.
(41) Zhou, Q.; Yang, C.; Zhao, Y. Dynamic Organic Room-Temperature Phosphorescent Systems. *Chem* **2023**, *9*, 2446–2480.
(42) Gao, H.; Ma, X. Recent Progress on Pure Organic Room Temperature Phosphorescent Polymers. *Aggregate* **2021**, *2*, e38.
(43) Kenry; Chen, C.; Liu, B. Enhancing the Performance of Pure Organic Room-Temperature Phosphorescent Luminophores. *Nat. Commun.* **2019**, *10*, 2111.
(44) Baumgartner, T. Insights on the Design and Electron-Acceptor Properties of Conjugated Organophosphorus Materials. *Acc. Chem. Res.* **2014**, *47*, 1613–1622.
(45) Yang, B.; Yan, S.; Li, C.; Ma, H.; Feng, F.; Zhang, Y.; Huang, W. Mn(Iii)-Mediated C-P Bond Activation of Diphosphines: Toward a Highly Emissive Phosphahelicene Cation Scaffold and Modulated Circularly Polarized Luminescence. *Chem. Sci.* **2023**, *14*, 10446–10457.
(46) She, P.; Qin, Y.; Zhou, Y.; Zheng, X.; Li, F.; Liu, S.; Ma, Y.; Zhao, Q.; Wong, W.-Y. Photoactivated Circularly Polarized Luminescent Organic Radicals in Doped Amorphous Polymer. *Angew. Chem. Int. Ed.* **2024**, *63*, e202403660.
(47) Xie, Z.; Mao, Z.; Wang, H.; Xiao, Y.; Zhang, X.; Yu, T.; An, Z.; Huang, W. Dual-Channel Mechano-Phosphorescence: A Combined Locking Effect with Twisted Molecular Structures and Robust Interactions. *Light Sci. Appl.* **2024**, *13*.
(48) Tao, Y.; Liu, C.; Xiang, Y.; Wang, Z.; Xue, X.; Li, P.; Li, H.; Xie, G.; Huang, W.; Chen, R. Resonance-Induced Stimuli-Responsive Capacity Modulation of Organic Ultralong Room Temperature Phosphorescence. *J. Am. Chem. Soc.* **2022**, *144*, 6946–6953.
(49) Das, B.; Makol, A.; Kundu, S. Phosphorus Radicals and Radical Ions. *Dalt. Trans.* **2022**, *51*, 12404–12426.
(50) Rosenboom, J.; Taube, F.; Teichmeier, L.; Villinger, A.; Reinhard, M.; Demeshko, S.; Bennati, M.; Bresien, J.; Corzilius, B.; Schulz, A. Rational Design of a Phosphorus-Centered Disbiradical. *Angew. Chem. Int. Ed.* **2024**, *63*.
(51) Tang, C.; Song, L.; Zhou, K.; Ren, P.; Zhao, E.; He, Z. Manipulating D-A Interaction to Achieve Stable Photoinduced Organic Radicals in Triphenylphosphine Crystals. *Chem. Sci.* **2023**, *14*, 1871–1877.
(52) Zhao, X.; Gong, J.; Alam, P.; Ma, C.; Wang, Y.; Guo, J.; Zeng, Z.; He, Z.; Sung, H. H. Y.; Williams, I. D.; Wong, K. S.; Chen, S.; Lam, J. W. Y.; Zhao, Z.; Tang, B. Z. A Simple Approach to Achieve Organic Radicals with Unusual Solid-State Emission and Persistent Stability. *CCS Chem.* **2022**, *4*, 1912–1920.
(53) Abe, M. Diradicals. *Chem. Rev.* **2013**, *113*, 7011−7088.
(54) Stuyver, T.; Chen, B.; Zeng, T.; Geerlings, P.; De Proft, F.; Hoffmann, R. Do Diradicals Behave like Radicals? *Chem. Rev.* **2019**, *119*, 11291–11351.
(55) Punzi, A.; Dai, Y.; Dibenedetto, C. N.; Mesto, E.; Schingaro, E.; Ullrich, T.; Striccoli, M.; Guldi, D. M.; Negri, F.; Farinola, G. M.; Blasi, D. Dark State of the Thiele Hydrocarbon: Efficient Solvatochromic Emission from a Nonpolar Centrosymmetric Singlet Diradicaloid. *J. Am. Chem. Soc.* **2023**, *145*, 20229–20241.
(56) Zhao, F.; Zhao, J.; Liu, H.; Wang, Y.; Duan, J.; Li, C.; Di, J.; Zhang, N.; Zheng, X.; Chen, P. Synthesis of π-Conjugated Chiral Organoborane Macrocycles with Blue to Near-Infrared Emissions and the Diradical Character of Cations. *J. Am. Chem. Soc.* **2023**, *145*, 10092–10103.
(57) Wu, H.; Hanayama, H.; Coehlo, M.; Gu, Y.; Wu, Z. H.; Takebayashi, S.; Jakob, G.; Vasylevskyi, S.; Schollmeyer, D.; Kläui, M.; Pieters, G.; Baumgarten, M.; Müllen, K.; Narita, A.; Qiu, Z. Stable π-Extended Thio[7]Helicene-Based Diradical with Predominant Through-Space Spin-Spin Coupling. *J. Am. Chem. Soc.* **2024**, *146*, 7480–7486.
(58) Hsieh, Y. C.; Wu, C. F.; Chen, Y. T.; Fang, C. Te; Wang, C. S.; Li, C. H.; Chen, L. Y.; Cheng, M. J.; Chueh, C. C.; Chou, P. T.; Wu, Y. T. 5,14-Diaryldiindeno[2,1-f:1′,2′-j]Picene: A New Stable [7]Helicene with a Partial Biradical Character. *J. Am. Chem. Soc.* **2018**, *140*, 14357–14366.
(59) Fabri, B.; Funaioli, T.; Frédéric, L.; Elsner, C.; Bordignon, E.; Zinna, F.; Di Bari, L.; Pescitelli, G.; Lacour, J. Triple Para-Functionalized Cations and Neutral Radicals of Enantiopure Diaza[4]Helicenes. *J. Am. Chem. Soc.* **2024**, *146*, 8308–8319.
(60) Shu, C.; Zhang, H.; Olankitwanit, A.; Rajca, S.; Rajca, A. High-Spin Diradical Dication of Chiral π-Conjugated Double Helical Molecule. *J. Am. Chem. Soc.* **2019**, *141*, 17287–17294.
(61) Ager, D. J.; East, M. B.; Eisenstadt, A.; Laneman, S. A. Convenient and Direct Preparation of Tertiary Phosphines via Nickel-Catalysed Cross-Coupling. *Chem. Commun.* **1997**, 2359–2360.
(62) Li, G.; Xu, K.; Zheng, J.; Fang, X.; Lou, W.; Zhan, F.; Deng, C.; Yang, Y. F.; Zhang, Q.; She, Y. High-Performance Ultraviolet Organic Light-Emitting Diodes Enabled by Double Boron-Oxygen-Embedded Benzo[m]Tetraphene Emitters. *J. Am. Chem. Soc.* **2024**, *146*, 1667–1680.
(63) Yang, J.; Guo, Q.; Wang, J.; Ren, Z.; Chen, J.; Peng, Q.; Ma, D.; Li, Z. Rational Molecular Design for Efficient Exciton Harvesting, and Deep-Blue OLED Application. *Adv. Opt. Mater.* **2018**, *6*, 1800342.
(64) Li, G.; Li, B.; Zhang, H.; Guo, X.; Lin, C.; Chen, K.; Wang, Z.; Ma, D.; Tang, B. Z. Efficient Ultraviolet Organic Light-Emitting Diodes with a CIEy of 0.04 and Negligible-Efficiency Roll-Off. *ACS Appl. Mater. Interfaces* **2022**, *14*, 10627–10636.
(65) Lu, T.; Chen, F. Multiwfn: A Multifunctional Wavefunction Analyzer. *J. Comput. Chem.* **2012**, *33*, 580–592.
(66) Beránek, T.; Jakubec, M.; Sýkora, J.; Císařová, I.; Žádný, J.; Storch, J. Synthesis of 2-Phospha[7]Helicene, a Helicene with a Terminal Phosphinine Ring. *Org. Lett.* **2022**, *24*, 4756–4761.
(67) Usui, K.; Narita, N.; Eto, R.; Suzuki, S.; Yokoo, A.; Yamamoto, K.; Igawa, K.; Iizuka, N.; Mimura, Y.; Umeno, T.; Matsumoto, S.; Hasegawa, M.; Tomooka, K.; Imai, Y.; Karasawa, S. Oxidation of an Internal-Edge-Substituted [5]Helicene-Derived Phosphine Synchronously Enhances Circularly Polarized Luminescence. *Chem. – A Eur. J.* **2022**, *28*, e202202922.
(68) Li, M.; Li, S. H.; Zhang, D.; Cai, M.; Duan, L.; Fung, M. K.; Chen, C. F. Stable Enantiomers Displaying Thermally Activated Delayed Fluorescence: Efficient OLEDs with Circularly Polarized Electroluminescence. *Angew. Chem. Int. Ed.* **2018**, *57*, 2889–2893.
(69) Qiu, W.; Liu, D.; Chen, Z.; Gan, Y.; Xiao, S.; Peng, X.; Zhang, D.; Cai, X.; Li, M.; Xie, W.; Sun, G.; Jiao, Y.; Gu, Q.; Ma, D.; Su, S. J. Afterglow OLEDs Incorporating Bright Closely Stacked Molecular Dimers with Ultra-Long Thermally Activated Delayed Fluorescence. *Matter* **2023**, *6*, 1231–1248.
(70) Wu, X.; Huang, J. W.; Su, B. K.; Wang, S.; Yuan, L.; Zheng, W. Q.; Zhang, H.; Zheng, Y. X.; Zhu, W.; Chou, P. T. Fabrication of Circularly Polarized MR-TADF Emitters with Asymmetrical Peripheral-Lock Enhancing Helical B/N-Doped Nanographenes. *Adv. Mater.* **2022**, *34*, 2105080.
(71) Yang, S. Y.; Wang, Y. K.; Peng, C. C.; Wu, Z. G.; Yuan, S.; Yu, Y. J.; Li, H.; Wang, T. T.; Li, H. C.; Zheng, Y. X.; Jiang, Z. Q.; Liao, L. S. Circularly Polarized Thermally Activated Delayed Fluorescence Emitters in Through-Space Charge Transfer on Asymmetric Spiro Skeletons. *J. Am. Chem. Soc.* **2020**, *142*, 17756–17765.
(72) Saal, F.; Swain, A.; Schmiedel, A.; Holzapfel, M.; Lambert, C.; Ravat, P. Push-Pull [7]Helicene Diimide: Excited-State Charge Transfer and Solvatochromic Circularly Polarised Luminescence. *Chem. Commun.* **2023**, *59*, 14005–14008.
(73) Shi, Y.; Li, C.; Di, J.; Xue, Y.; Jia, Y.; Duan, J.; Hu, X.; Tian, Y.; Li, Y.; Sun, C.; Zhang, N.; Xiong, Y.; Jin, T.; Chen, P. Polycationic Open-Shell Cyclophanes: Synthesis of Electron-Rich Chiral Macrocycles, and Redox-Dependent Electronic States. *Angew. Chem. Int. Ed.* **2024**, DOI:10.1002/anie.202402800.
(74) Ni, Y.; Gopalakrishna, T. Y.; Phan, H.; Kim, T.; Herng, T. S.; Han, Y.; Tao, T.; Ding, J.; Kim, D.; Wu, J. 3D Global Aromaticity in a Fully Conjugated Diradicaloid Cage at Different Oxidation States. *Nat. Chem.* **2020**, *12*, 242–248.
(75) Yang, B.; Yan, S.; Ban, S.; Zhang, Y.; Ma, H.; Huang, W. Topology-Directed Synthesis of Helical Phosphoniums with High Diradical Character and Polar-Dependent Electron Transfer. *ChemRxiv* **2024**, https://doi.org/10.26434/chemrxiv-2024-clvm4.